Contrib Mineral Petrol (1999) 137: 36–45

P. Bottazzi · M. Tiepolo · R. Vannucci · A. Zanetti
R. Brumm · S.F. Foley · R. Oberti

Distinct site preferences for heavy and light REE in amphibole and the prediction of $^{Amph/L}D_{REE}$

Received: 17 March 1999 / Accepted: 11 June 1999

Abstract New experimental amphibole/melt partition coefficients from a variety of geologically relevant amphibole (pargasite, kaersutite, and K-richterite) and melt compositions obtained under conditions of interest to upper-mantle studies are combined with the results of X-ray single-crystal structure refinement. The ideal cation radii (r_0), calculated using the lattice-site elastic-strain model of Blundy and Wood (1994) under the hypothesis of complete REE (rare earth elements) ordering at $^{[8]}$M4, mostly differ significantly from those obtained from both the structure refinement and the ionic radius of $^{[8]}Ca^{2+}$. Heavier REE may also strongly deviate from the parabolic trends defined by the other REE. On the basis of the crystal-chemical knowledge of major-element site-preference in amphibole and the occurrence of two sites with different co-ordination within the M4 cavity (M4 for Ca and Na, M4′ for Fe^{2+} and Mg), we propose a new model for REE incorporation. LREE order at the $^{[8]}$M4 site, whereas HREE prefer the M4′ site with lower co-ordination in amphiboles with a significant cummingtonite component, and may also enter the M2 octahedron, at least in richterite. This more complex model is consistent with the observed $^{Amph/L}D$, and drops the usual assumption that REE behave as a homogeneous group and order at the M4 site. The availability of multiple crystal-chemical mechanisms for REE^{3+} incorporation explains why measured and estimated $^{Amph/L}D_{HREE}$ may differ by up to one order of magnitude. When REE enter two different sites within the same cavity, a fit performed on the basis of a single curve may appear correct, but the values obtained for r_0 are biased towards those of the dominant site, and the Young's modulus is underestimated. When REE are incorporated in multiple sites in different cavities, the observed pattern cannot be reduced to a single curve, and the partition coefficients of heavy REE would be strongly underestimated by a single-site fit. The simplistic assumption that REE occupy a single site within the amphibole structure can thus substantially bias predictive models based on the elastic-strain theory. Our combined approach allows linkage between fine-scale site preference and the macroscopic properties of minerals and provides more reliable predictive models for mineral/melt partitioning. After the possible site-assignments have been identified, the shape of the Onuma curves constructed from accurately determined $^{Amph/L}D_{REE}$ now allows the active mechanisms for REE incorporation in amphiboles to be recognised even where site populations are not available. The REE preference for polyhedra with smaller size and lower co-ordination than those occupied by Ca invalidates the general idea that Ca acts as a "carrier" for REE.

P. Bottazzi (✉) · R. Vannucci · A. Zanetti · R. Oberti
CNR-Centro di Studio per la Cristallochimica e la Cristallografia (CSCC), Via Ferrata 1, I-27100 Pavia, Italy

M. Tiepolo · R. Vannucci
Dipartimento di Scienze della Terra, Università di Pavia, Via Ferrata 1, I-27100 Pavia, Italy

R. Brumm · S.F. Foley
Mineralogisch-Petrologisches Institut, Universität Göttingen, Goldschmidtstrasse 1, D-37077 Göttingen, Germany
E-mail: sfoley@gwdg.de

Editorial responsibility: J. Hoefs

Introduction

Current knowledge of the residence of rare earth elements (REE) indicates that lighter REE are mostly hosted in Ca-bearing, rock-forming minerals with large or intermediately sized polyhedra, such as clinopyroxene, amphibole, apatite and epidote. This has led to the general assumption that all the REE^{3+} substitute for Ca in eight-fold co-ordinated polyhedra in such minerals, despite the fact that Ca-poor minerals (e.g. zircon, pyrope garnet, orthopyroxene) are strongly selective in their uptake of heavier REE. The "carrier function" of REE by Ca, however, is supported by the positive correlation between the concentration of Ca and the

partition coefficients of trivalent REE reported in clinopyroxene (Harte and Kirkley 1997; Hack et al. 1994).

The dependence of REE partitioning behaviour on the physical characteristics of the structural sites available in each mineral has been the subject of several studies. Blundy and Wood (1994) and Wood and Blundy (1997) modelled the influence of the crystal structure on the basis of the size and elasticity of the relevant co-ordination polyhedra. Their starting point is the equation proposed by Brice (1975), which relates the energy stored in the crystal structure upon the substitution of a cation for a homovalent "ideal" cation (for which the strain is zero) to the difference in their ionic radii and to the Young's modulus of the co-ordination polyhedron in which the substitution takes place. An equivalent approach was also proposed by Beattie (1994), based on the work of Nagasawa (1966). The two models were later shown to be numerically equivalent within ~10% (Purton et al. 1996). The aim of both approaches was to quantify the observations of Onuma et al. (1968) that the partition coefficients are highest for chemical species with ionic radii closest to that of the dominant constituent with the same co-ordination number. These approaches have been successfully applied to predict partition coefficients for REE^{3+} and other trace elements in clinopyroxene (Wood and Blundy 1997) and olivine (Beattie 1994) at a given P, T and bulk composition. In these and other studies, attention was focused on REE^{3+}, not only because of their geochemical importance but also due to the fact that they are considered a homogeneous geochemical series not internally discriminated by the melt structure (Ryerson and Hess 1978).

Fewer experimental studies have focused on amphibole (Dalpé and Baker 1994; Adam and Green 1994; Sweeney et al. 1992; Andreessen et al. 1996; Brenan et al. 1995; LaTourrette et al. 1995; Klein et al. 1997), despite its wide occurrence and ability to incorporate larger amounts of geochemically relevant trace elements than clinopyroxene (e.g. Wood and Blundy 1997, and references therein). This is partly because clinopyroxene is expected to exert a dominant control on REE partitioning in most geologic environments, and partly because of the experimental difficulty of stabilising amphibole near the liquidus.

The crystal-chemical control on REE^{3+} partitioning between amphibole and melt is even more poorly known, and is usually inferred from considerations based on the geochemical coherence of REE and Ca and on the similarity of the M4 site in amphibole to the M2 site in clinopyroxene. Accordingly, the relationship between amphibole/melt partition coefficients ($^{Amph/L}D$) and the crystal structure has so far been modelled using the elastic-strain model of Blundy and Wood (1994), assuming that all REE^{3+} order at the eight-fold co-ordinated M4 site (Brenan et al. 1995; LaTourrette et al. 1995).

In order to provide a better understanding of the mechanisms of trace-element incorporation in amphibole and of their ordering patterns, we performed new mineral/melt partitioning experiments for a wide range of amphibole compositions and 33 trace elements. The information derived from the application of the lattice-site elastic-strain theory of Blundy and Wood (1994) to the measured partition coefficients was combined with the results of structure refinement (SREF) performed on the same experimentally synthesised amphibole crystals.

In this paper, we report a selection of samples which is representative of the distinct site preferences for the incorporation of REE in various amphibole compositions, and discuss the implications of the inferred REE ordering patterns for the prediction of partitioning between amphibole and melt. Discussion of the mechanisms of incorporation of other trace elements will be reported elsewhere (Brumm et al. 1999; Foley et al. 1999; Oberti et al. 1999a; Tiepolo et al., unpublished).

A crystal-chemical framework for the interpretation of REE behaviour in amphibole

In previous studies, heavy and light REE^{3+} in amphiboles have been assigned, together with Ca^{2+}, exclusively to the $^{[8]}$M4 site. The cation ordering in the M4 cavity (Fig. 1) is, however, rather complex because it is surrounded by eight oxygen and can be occupied by several major-element cations with very different eight-fold co-ordinated ionic radii (Shannon 1976). Na (ionic radius 1.18 Å), Li (0.92 Å), Ca (1.12 Å), Mn^{2+} (0.96 Å), Fe^{2+} (0.92 Å), and Mg (0.89 Å), Sr (1.26 Å) and K (1.51 Å) have been reported with full occupancy in synthetic K-richterite, although the latter has been found only at very high P (15 GPa; Yang et al. 1999). Therefore, when different cations are incorporated into the M4 cavity, the individual polyhedra throughout the crystals may be very different in size. The structure refinement can only give an image of the structure averaged over the whole crystal, but important information on local configurations can be obtained also from this averaged picture.

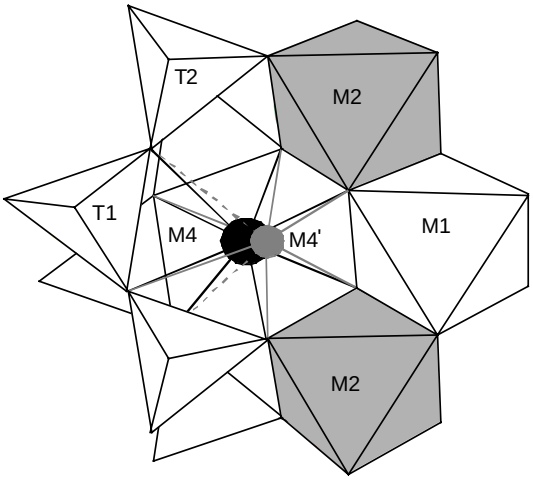

Fig. 1 Detailed environment of part of the amphibole structure showing the sites relevant to the present discussion

If different cations occur at a fixed position in the cavity, the co-ordinated oxygen may move toward or away from the central cation as a function of its ionic radius. Their resulting electron-density maxima elongate in the direction of the central cation, and this situation is modelled during structure refinement by high and strongly anisotropic atomic-displacement parameters (adp) or even by slightly different atomic positions, only one of which is locally occupied by oxygen. In the framework of the elastic-strain model, this situation can be regarded as the "relaxation" of the oxygen around the cation which underwent substitution.

If the oxygen framework is kept fixed by the other structural sites and the cations order at different positions as a function of their ionic radius, then the electron density within the cavity elongates along the preferential direction of the ordering. This is the prevailing situation observed for the M4 cations in amphiboles. The electron-density maximum of M4 cations in amphiboles is nearly always asymmetrical, sometimes very strongly so, and Fourier maps allow the detection of a splitting into two different positions. Therefore, two distinct sites (M4 for Ca and Na, M4′ for the smaller cations) are usually inserted in the model and refined with the total occupancy fixed to 1.0. In the case of Ca and Fe^{2+}, the separation between the two sites is close to the resolution of the standard set of data, and thus the co-ordinates of the (usually less populated) M4′ site cannot be determined with high accuracy. However, a number of works based on structure refinement have shown that the M4 and M4′ sites are aligned along the binary axis with y/b values varying continuously from 0.23 (Mg) to 0.28 (K) as a function of the increasing ionic radius of the constituents (see Oberti and Ghose 1993 for references). When Li and Mg are present at the M4 site, the distance to the two O5 oxygen atoms becomes much longer than 3 Å, but significant changes in the co-ordinating shell also occur for Mn and Fe^{2+}. The changes in co-ordination thus depend on both the nature of the M4 cations and the composition of the adjacent structural sites. For example, the environment differs for Mg between cummingtonite (no $^{[4]}$Al) and pargasite (2 $^{[4]}$Al pfu) because of the distortion of the tetrahedral chains that form one wall of the cavity. In all such cases, this behaviour is too complex and has not been modelled as a simple relaxation of the oxygen framework.

The simultaneous presence of M4 polyhedra with very different sizes and distortion is difficult for the structure to accommodate, especially under low-temperature conditions. The amount of small cations at M4 does not normally exceed 0.10 apfu, and exsolution lamellae and other microstructures are often observed in crystals that have re-equilibrated at lower temperature. However, the fraction of Mg, Fe and Mn (cummingtonite component) occurring in the M4 cavity in Na-Ca amphiboles may become significant (0.20–0.50 apfu) at high temperature. It has been reported to reach 1.0 apfu in synthetic "sodic" amphiboles crystallised in a Ca-free system and quenched from 800–840 °C (Oberti et al. 1999b). The cummingtonite component is thus important in studies of upper-mantle assemblages, and is present in nearly all amphiboles in our set of experiments. The availability of two sites within the M4 cavity and the difference in size and co-ordination of the resulting polyhedra imply differing behaviour with respect to REE incorporation.

Other sites in the amphibole structure are not usually considered relevant to REE partitioning; in particular, the possibility that REE^{3+} may enter octahedra is generally neglected. However, it cannot be discarded in principle, especially for the heavier REE, on the basis of both ionic radii (Lu = 0.86 Å, Yb = 0.87 Å in six-fold co-ordination) and ionic charge. Elements with large radii, both divalent (Mn, 0.83 Å) and trivalent (Sc, 0.745 Å and In, 0.80 Å), are known as major constituents in amphibole, especially in richterite, where the octahedral strip is particularly enlarged due to effects from the other structural sites.

Experimental

Synthesis experiments

Results are presented here for amphibole/melt partitioning experiments in three different systems in which amphibole crystallised as a near-liquidus constituent. These are an alkali-olivine basalt (AOB) from Hessen, Germany (Wedepohl 1983), a lamproite (LAM) from melting experiments on mica-amphibole-rutile-ilmenite-diopside (MARID)-like assemblages (Foley et al. 1996; van der Laan and Foley 1994), and an ultramafic lamprophyre (UML) from the Jetty Peninsula, Antarctica (Andronikov and Egorov 1993). The natural compositions were also reproduced as oxide mixtures and varied in different runs along the compositional vectors $K_2O/(Na_2O + K_2O)$, $MgO/(MgO + FeO)$ and $TiO_2/(TiO_2 + SiO_2)$. All the synthetic starting compositions were doped with 33 trace elements, including REE (rare earth elements), LILE (large ion lithophile elements), HFSE (high field strength elements) and some transition elements. REE concentrations were increased to between 70 ppm for LREE and 555 ppm for the HREE in order to minimise molecular interference during secondary ion mass spectrometry (SIMS) analyses and to optimise counting statistics to better than 2%. Experiments were carried out at the University of Göttingen using a 22-mm piston-cylinder apparatus with a CaF_2-assembly and graphite-lined Pt-capsules. Amphibole crystallisation under conditions relevant to mantle processes (1.4 GPa pressure) was promoted by adding water. The water contents in the glasses were determined by SIMS to be lower than 5 wt%. All the amphiboles were found to be partially dehydrogenated, as expected for upper-mantle assemblages. All charges were brought to superliquidus conditions (1270 °C) for 1 h and then cooled at rates of 1–0.5 °C/min to the equilibrium temperature (T_{eq}), at which they were kept for 13–27 h before quenching. The oxygen fugacity was buffered by the inner graphite capsule, leading to a Δ(FMQ) of −2.

Analytical techniques

Amphibole/glass pairs were characterised for major elements by electron microprobe at the Centro Grandi Strumenti of the Università di Pavia. Trace and volatile (H, F, Cl) elements were determined by ion probe at the CNR-CSCC (Centro di Studio per la Cristallochimica e la Cristallografia) on spots of 20–25 μm diameter, and using ^{30}Si as the internal standard. Other methodological details can be found in Bottazzi et al. (1994) and Ottolini et al.

(1995). The error on determinations of cation concentrations is approximately 10%. As systematic effects are basically removed in the amphibole/glass ratios, and matrix effects are negligible with these amphibole and glass compositions, the accuracy in determining the concentration ratios is estimated to be smaller than 10%, and larger than that due to counting statistics and the reproducibility limit.

In the products of the undoped experiments, all REE were analysed by laser ablation microprobe – inductively coupled plasma – mass spectrometry (LAM–ICP–MS). These first results from the CNR–CSCC laser probe in Pavia were obtained using a pulsed Nd:YAG laser source "Brilliant" (Quantel, Les Ulis, France), in which the fundamental emission in the infrared (1064 nm) is converted into ultraviolet radiation (266 nm) by means of two harmonic generators. The system was developed at the Memorial University of Newfoundland (MUN), and its basic design and operation are described in Taylor et al. (1997). The energy of the laser pulse can be continuously varied by means of an energy attenuator and the diameter of the ablation crater by defocusing the laser beam.

For the present work, the laser was operated at a repetition rate of 10 Hz, and the spot diameter was ~40 μm with a pulse energy of about 0.07 mJ. The particles produced by ablation were analysed by a field-sector mass spectrometer ("Element", Finnigan MAT, Bremen, Germany). An RF power of 1300 W was used, and the Ar gas flows into the ICP torch were as follows: sample; 1.35 l min^{-1}, auxiliary; 1.0 l min^{-1} and coolant; 13 l min^{-1}. A total of 34 peaks were acquired at a mass resolving power of ~350 by peak jumping between the masses of interest. At each mass, a mass window slightly larger than the peak width was scanned and the intensity was averaged over the full peak-width. Ablation signal integration intervals were selected by carefully inspecting the time-resolved analysis to ensure that no inclusions were present in the analysed volume, and data reduction was performed by the software package "LamTrace" developed at MUN, using the method described by Longerich et al. (1996). NIST SRM 612 was used as the external standard, and ^{44}Ca as the internal standard. Reproducibility and accuracy of the REE concentrations were assessed on the control sample BCR2-g (MUN, ICP-MS, unpublished data) to be approximately <7 and 10%, respectively.

At least one crystal of suitable size for X-ray single-crystal structure refinement (SREF) was extracted from each experimental charge by hand picking after grinding. The quality of the crystals and the absence of inclusions were checked by optical microscopy and by the profile of selected Bragg reflections. The procedures for X-ray analysis, data collection and refinement are those reported in Oberti et al. (1992). The refinements converged to R_{obs} 1–2% and thus yielded very accurate values for interatomic distances and site scattering. All the results were critically examined and compared to the amphibole database at the CNR–CSCC, which presently hosts complete chemical and structural characterisation of more than 950 amphibole compositions, and allows detailed modelling of amphibole crystal chemistry. Reliable site populations and cation partitioning for major elements could thus be obtained for the complex amphibole compositions of the present work. The present study is not intended to be a crystal-chemical work, therefore, only the relevant refinement results are presented in this report. Further details of the procedure can be found in Tiepolo et al. (1999) and Oberti et al. (1999a), and more results on the samples of this experimental series can be obtained from the authors (R.O. and A.Z.) upon request.

Results

The experiments yielded 100–200 μm amphibole crystals as the dominant phase. Olivine and clinopyroxene occur as accessory high temperature phases and occasionally within amphibole. Amphibole was the final phase in the crystallisation sequence. The degree of crystallisation in all experiments was estimated to be less than 50% from major-element mass balance. Crystals formed during quenching were scarce or absent in the glass. Homogeneity of amphibole and melt was checked by traverses across crystals and glass during the electron-microprobe analyses of the experimental products. Chemical homogeneity of both amphibole and glass as well as the euhedral shape of amphiboles suggest near-equilibrium conditions. Around 300 chemical and 60 structural characterisations of amphibole crystals were obtained; however, for clarity only the results obtained on three selected amphiboles which are representative of the REE^{3+} patterns observed in the whole data set are reported. This also allows the discussion of the possible mechanisms of REE incorporation. The selected samples are: (1) a kaersutite with a high cummingtonite component [0.35 (Mg, Fe^{2+}) apfu in the M4 cavity], kae 4722–13a; (2) a pargasite with a very low cummingtonite component [<0.02 ^{M4}(Mg, Fe^{2+}) apfu], par RB52–3 and (3) a K-richterite with no cummingtonite component, K-ric RB31–1 (Table 1). $^{Amph/L}D_{REE}$ measured for all other synthetic amphiboles are reported and discussed elsewhere (Brumm 1998; Tiepolo 1999). The samples are referred to by the sample names indicated above to emphasize that the behaviour described for each may not necessarily apply to all amphiboles formally classified as K-richterite, pargasite or kaersutite.

The charge distribution is only one of the two main factors determining REE incorporation, the other being the amount of the cummingtonite component. The content of the cummingtonite component estimated from chemical analyses is in agreement with that determined by SREF analysis. The geometrical characterisation of both the M4 and M4′ sites could be obtained for kae 4722–13a, whereas the shape of the electron density in the M4 cavity allowed exclusion of significant (>0.02 apfu) Fe and Mg in the other two samples.

REE^{3+} partition coefficients for the three selected crystals (Table 2 and Fig. 2) vary by nearly one order and two orders of magnitude for light REE and heavy REE respectively. In general, an increase in $^{Amph/L}D$ is observed going from K-richterite through pargasite to kaersutite. Note that D_{Dy}, D_{Er} and D_{Yb} lie on the trend defined by the D values for the other REE in kae 4722–13a, but deviate substantially from this trend in K-ric RB31–1, whereas D_{Yb} is nearly one order of magnitude higher than D_{Dy}. A slight deviation is also observed for par RB52–3, where Yb and Er have nearly identical partition coefficients.

Detailed comparison of the REE partition coefficients of the three selected samples with those from previous studies is beyond the scope of this paper. It is only noted that there is overall consistency of the $^{Amph/L}D$ patterns for the two calcic amphiboles with other data available for basaltic to andesitic systems (Dalpé and Baker 1994; Andreessen et al. 1996; LaTourrette et al. 1995). Other data for richterite are not available to our knowledge, however, the lower D_{REE} values observed in K-ric

Table 1 Major element compositions of the three amphiboles selected for their representative behaviours towards REE incorporation. Major-element oxides (wt%) determined by electron microprobe, H and F by SIMS

Sample	4722–13a Kae	RB52–3 Par	RB31–1 K–ric
Starting material	AOB	UML	LAM
Teq (°C)	1015	950	850
SiO_2	40.72	39.72	54.04
TiO_2	4.06	1.40	1.64
Al_2O_3	15.02	17.09	0.52
Cr_2O_3	0.01	0.07	0.05
FeO_T	8.62	7.73	7.94
MnO	0.12	0.01	0.00
MgO	14.48	15.02	18.79
CaO	10.51	12.98	5.93
Na_2O	2.59	2.60	4.17
K_2O	1.33	1.28	4.75
H_2O	1.13	1.83	2.07
F	0.18	0.00	0.02
—O=F	0.08	0.00	0.01
Σ	98.70	99.73	99.91
Unit formulae (apfu)			
Si	6.013	5.756	7.758
Al	1.987	2.244	0.088
Ti	0.000	0.000	0.154
ΣT	8.000	8.000	8.000
Al	0.629	0.676	0.000
Fe^{3+}	0.248	0.453	0.194
Ti	0.450	0.153	0.023
Cr	0.002	0.008	0.006
Mg	2.998	3.242	4.018
Fe^{2+}	0.673	0.468	0.759
ΣM(1,2,3)	5.000	5.000	5.000
Mg	0.186	0.000	0.000
Fe^{2+}	0.143	0.016	0.000
Mn^{2+}	0.015	0.001	0.000
Ca	1.656	1.983	0.912
Na	0.000	0.000	1.088
ΣM4	2.000	2.000	2.000
Ca	0.007	0.033	0.000
Na	0.742	0.730	0.073
K	0.251	0.237	0.870
ΣA	1.000	1.000	0.943
OH	1.116	1.769	1.981
F	0.084	0.000	0.005
O	0.800	0.231	0.014
ΣX	2.000	2.000	2.000

Table 2 Trace-element concentrations and calculated partition coefficients for the three representative amphiboles. Partition coefficients are calculated from average amphibole and glass concentrations

Elements	4722–13a Kae[a]	RB52–3 Par[b]	RB31–1 K–ric[c]
Average trace-element concentrations (ppm)			
La	13.5	8.48	7.15
Ce	38.8	9.41	8.45
Pr	5.92	–	–
Nd	28.9	11.8	7.63
Sm	7.59	40.3	13.2
Eu	2.53	78.8	39.0
Gd	6.94	76.6	13.0
Tb	0.98	–	–
Dy	5.07	143	16.8
Ho	0.84	–	–
Y	19.4	–	5.56
Er	2.13	178	37.9
Tm	0.24	–	–
Yb	1.48	322	179
Lu	0.18	–	–
V	–	–	698
Sc	–	–	2300
Amphibole/liquid partition coefficients			
La	0.116	0.0437	0.0274
Ce	0.185	0.0709	0.0293
Pr	0.277	–	–
Nd	0.396	0.123	0.0325
Sm	0.651	0.158	0.0240
Eu	0.657	0.175	0.0498
Gd	0.933	0.188	0.0180
Tb	1.00	–	–
Dy	0.967	0.165	0.0136
Ho	1.03	–	–
Y	0.873	–	0.0196
Er	0.851	0.175	0.0318
Tm	0.816	–	–
Yb	0.787	0.177	0.102
Lu	0.698	–	–
V	–	–	3.67
Sc	–	–	7.43

[a] Average of three amphibole analyses by LAM–ICP–MS; standard deviations (1σ) of partition coefficients range from 3 to 10%, except for Lu (21%)
[b] Average of two amphibole analyses by SIMS; 1σ less than 7%
[c] Average of two amphibole analyses by SIMS; 1σ from 4 to 17%, except for Yb (30%)

RB31–1 are consistent with the expected limited capability of K-ric for hosting trivalent cations at the major-element level. The lower values are also consistent with the presence of Na in more than half of the K-ric RB31–1 M4 sites (this would imply local jumps of +2 in the ionic charge).

Ideal cation radii (r_0), Young's moduli (E), and "strain-compensated partition coefficients" (D_0) were calculated by least-squares fitting of the measured partition coefficients to the theoretical curve given by Eq. (2) of Blundy and Wood (1994). Firstly, fits were carried out assuming that all REE^{3+} order at the $^{[8]}$M4 position. Dy, Er and Yb were excluded in K-ric RB31–1 due to their systematic deviation from the parabolic trend. In par RB52–2, the similarity of D_{Yb} and D_{Er} resulted in unrealistically short r_0 and small E values, and they were thus excluded from the fit. The results are reported in Table 3 and Fig. 3.

An estimate of the long-range average ionic radius (r*) was obtained from the refined, mean bond lengths by subtracting 1.38 Å, the ionic radius of $^{[4]}O^{2-}$. The resulting r* values are 1.117 Å in par RB52–3, close to the ionic radius of $^{[8]}$Ca (1.12 Å), but only 1.107 Å in kae 4722–13a. The larger value of r* obtained for K-ric RB31–1 (1.192 Å) is in agreement with the presence of Na (ionic radius 1.18 Å; 1.08 apfu) and with the knowledge that the M4 polyhedra in richterites are larger than expected on the basis of their site populations.

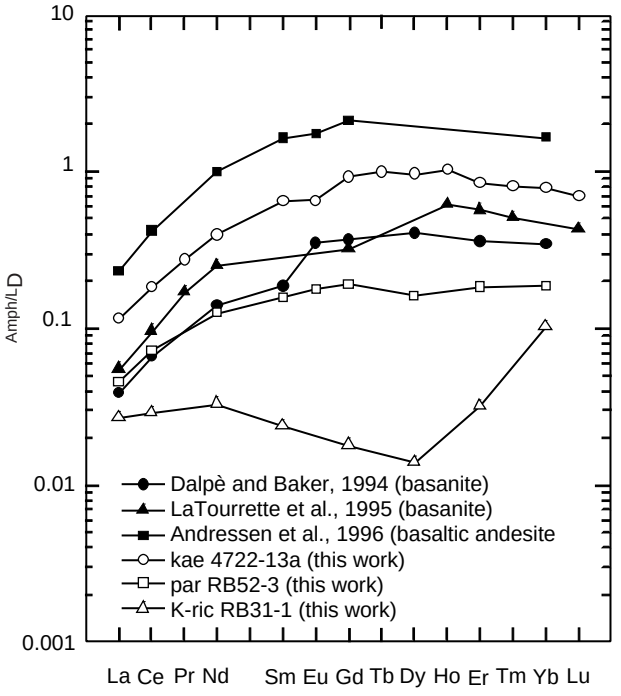

Fig. 2 Representative REE partition coefficients between amphibole and melt from the new experimental data set (*open symbols*). Experimentally determined values from previous studies for basaltic to andesitic systems (*filled symbols*) are shown for comparison

Discussion

Comparison of measured and calculated site dimensions

When addressing the issue of cation partitioning with such different approaches as the elastic-strain model and structure refinement, the first point to clarify is whether there should be a correspondence between r_0, the ionic radius of the ideal cation, and r*, the cation radius (the weighted average over all symmetry-related sites in the crystal), measured from SREF. If all these sites were equally available for REE incorporation, independently of the size of the actual constituent, r_0 should correspond to r*. However, the incorporation of REE may be restricted to those sites occupied by specific constituents, in which case r_0 should be close to the weighted average of the ionic radii of the cations occupying only those sites. The +2 change in the ionic charge resulting from substitution of REE for Na in a single M4 site can be less easily compensated by incorporation of lower-charge substituents in the adjacent structural sites [i.e. of vacancy for (Na, K) at the A site and of Al for Si at the T1 site], than can REE substitution after Ca (charge difference +1). It is thus likely that the M4 sites occupied by Na do not significantly contribute to REE incorporation and so, only the sites occupied by Ca should be considered. If this is true, then r_0 for REE in K-richterite should be closer to the ionic radius of Ca than to the value of r* obtained from ⟨M4–O⟩.

Table 3 Selected SREF and best-fit results for the three representative amphiboles

	4722–13a Kae	RB52–3 Par	RB31–1 K-Ric
Unit cell dimensions			
a (Å)	9.861	9.966	10.069
b	18.023	18.031	18.051
c	5.307	5.308	5.287
β (°)	105.21	105.62	104.79
Vol (Å)^3	910.1	918.7	929.1
Interatomic distances (Å)			
⟨T1–O⟩	1.670	1.677	1.623
⟨T2–O⟩	1.638	1.646	1.641
⟨M1–O⟩	2.079	2.087	2.082
⟨M2–O⟩	2.054	2.055	2.097
⟨M3–O⟩	2.072	2.071	2.080
⟨M4–O⟩ (8)	2.487	2.497	2.573
⟨M4′–O⟩(6)	2.417	–	–
⟨A–O⟩	2.931	2.939	2.957
Best-fit results[a]			
(1) $^{REE}r_0$ (Å)	1.028	1.052	1.123
D_0	0.98	0.18	0.032
E (GPa)	339	282	276
(2) $^{M4}r_0$ (Å)	1.12	–	–
$^{M4'}r_0$ (Å)	1.025	–	–
$^{M4}D_0$	0.12	–	–
$^{M4'}D_0$	0.97	–	–
$^{M4,M4'}$E (GPa)	469	–	–
(3) $^{M4}r_0$ (Å)	–	–	1.123
$^{M2}r_0$ (Å)	–	–	0.717
$^{M4}D_0$	–	–	0.033
$^{M2}D_0$	–	–	5.36
^{M4}E (GPa)	–	–	323
^{M2}E (GPa)	–	–	528

[a] Ideal cation radii calculated from REE partitioning data according to the model of Blundy and Wood (1994) using different assumptions for REE ordering: (1) all REE ordered at the M4 site; (2) REE distributed between the M4 and M4′ sites; (3) REE distributed between the M4 and M2 sites

The value of r_0 obtained for K-ric RB31–1 excluding the heavier REE from the single-site fit compares well with the ionic radius of Ca (Table 3 and Fig. 3). Thus the assumption that REE^{3+} replace only $^{[8]}$Ca in the M4 site is correct in the case of K-ric RB31–1 due to the negligible incorporation of REE^{3+} into the sites occupied by $^{[8]}$Na, and to the absence of the cummingtonite component. In this case, the elastic-strain model and the crystal-chemical evidence converge to the same result, supporting the hypothesis that r_0 corresponds to the actual dimension of only those sites available for REE^{3+} incorporation. The departure of the heavy REE from the bell-shaped trend is due to their incorporation at an octahedral site (see below).

In the case of kae 4722–13a, the occurrence of two sites within the M4 cavity adds further complexity and makes the application of the elastic-strain model less straightforward. If the M4 cavity is occupied by divalent cations smaller than Ca, its geometry becomes highly distorted and the co-ordination number tends to decrease. The small value of $^{[8]}r_0$ (1.028 Å), obtained by

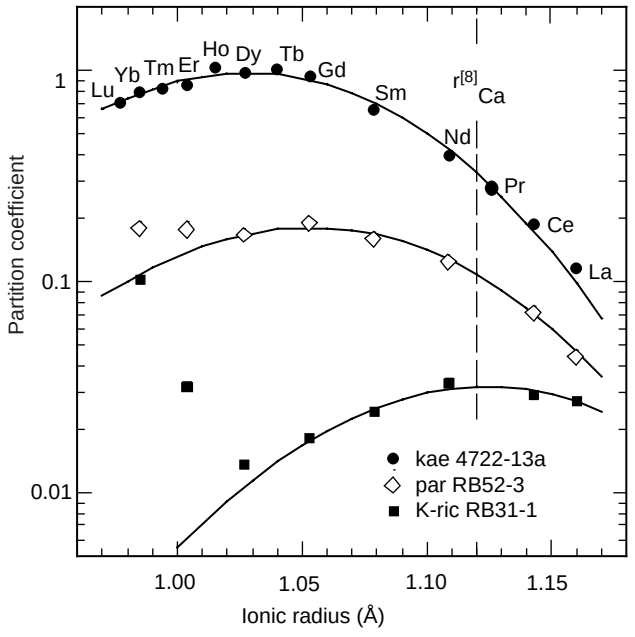

Fig. 3 Experimentally determined partition-coefficients for the three representative amphiboles versus cation radius. The curves represent single-site fits to Blundy and Wood's (1994) elastic-strain model (see Table 3) assuming ordering of all REE^{3+} at the $^{[8]}$M4 site. For pargasite, Yb and Er lie off the trend, whereas for K-richterite, all three of Yb, Er and Dy lie off the trend defined by the other REE. Note that the curve is centred close to the ionic radius of Ca in K-ric RB31–1, in which Na is the prevailing cation at M4, whereas it is centred at far shorter radii in par RB52–3 and kae 4722–13a in which Ca is the dominant cation at M4

fitting the data to a single curve, indicates that REE prefer smaller sites (i.e. M4′). When the six-fold co-ordinated ionic radii are used for REE, we obtain $^{[6]}r_0 = 0.91$ Å, which closely approaches the dimension of the six-fold co-ordinated M4 site obtained by structure refinement of Fe-cummingtonite. Therefore, in the case of the kae 4722–13a, REE seem to enter "cummingtonite-like" M4 sites faster than "pargasite-like" ones.

As this conclusion apparently contradicts results of the K-ric RB31–1, REE incorporation in amphiboles was modelled with a significant cummingtonite component by assuming that REE may be distributed between the two distinct sites in the M4 cavity. The shape of the pattern observed in kae 4722–13a does not allow fitting of two independent elastic-strain curves. However, the number of parameters can be reduced by the reasonable assumption that the Young's moduli of the M4 and M4′ polyhedra are equal. Eight-fold co-ordinated ionic radii for REE can be used for both curves, as the ionic radii of REE in six- and in eight-fold co-ordination are basically proportional (Shannon 1976). The effect on r_0 of the actual co-ordination of the smaller sites can be considered a posteriori from the comparison to the measured $^{M4'}r^*$. The resulting "double-site" fit for the kae 4722–13a (Table 3 and Fig. 4a) gives a value of $^{M4}r_0$ equal to 1.12 Å, which coincides with the $^{[8]}$Ca ionic radius and compares well with the observed $^{M4}r^*$ (1.107 Å). The value of 1.028 Å obtained for $^{[8]}r_0$ based on the hypothesis of a single M4 site can thus be explained by the fact that this model indicates the behaviour of the M4′ site, which dominates the incorporation of trivalent REE ($^{M4'}D_0$ is one order of magnitude higher than $^{M4}D_0$).

The trend observed for the HREE in K-ric RB31–1 (Fig. 3) cannot be reconciled with a single ordering pattern, and suggests that REE must also enter significantly smaller sites. The sharp break in the trend observed at about Dy is consistent with the occurrence of the heaviest REE on the steep edge of the relaxation curve of an octahedron, and we thus assumed that REE are incorporated in at least one of the three independent octahedra. The simultaneous fit of the measured D_{REE} to two curves, one relative to a six-fold and the other to an eight-fold co-ordinated site, gives r_0 for the former equal to 0.72 Å, typical of an octahedron occupied by Mg (Table 3 and Fig. 4b). The best candidate is the M2 site, because it is the largest octahedron in K-richterite and, therefore, the incorporation of trivalent cations may locally compensate the substitution of Al for Si at T1. The r_0 value obtained for the six-fold co-ordinated site in this fit agrees well with the measured $^{M2}r^*$ (0.717 Å). Furthermore, the measured D values for $^{[6]}Sc^{3+}$ and $^{[6]}V^{3+}$, which order at M2 as shown by SREF studies on synthetic amphiboles, are accurately predicted.

The assignment of HREE to the octahedral M2 site in K-ric RB31–1 has been made easier by the low value of $^{M4}D_0$ for trivalent cations and by the absence of a cummingtonite component. Moreover, the M2 polyhedron in K-richterite is likely to be more suitable for the incorporation of HREE (up to about Dy) than in kaersutite, where M2 is smaller due to the nearly stoichiometric incorporation of small trivalent cations.

It is thus proposed that REE are distributed over more than one structural site in amphibole, and that HREE (including middle REE) may prefer sites with co-ordination numbers lower than eight. Within each site, the difference between the ionic radius of the single REE and the ideal cation radii r_0 is a discriminating factor according to the elastic-strain model. The shape of the patterns observed for partition coefficients can thus be rationalised in terms of the different possibilities available for the incorporation of each REE (i.e. the frequency of the suitable sites in the crystal and their actual dimensions and compliance). The deviation from the expected curve on the left-hand side of the single-fit curve is roughly proportional to the cummingtonite component in the whole set of synthetic amphiboles of this work. We suggest that kae 41722–13a and K-ric RB31–1 (Fig. 4a, b) can be considered as "end members" with respect to the ordering of REE in amphibole. In the kae 41722–13a, the pattern is dominated by the M4′ site, whereas in the K-ric RB31–1, the large M2 octahedron is more suitable for the incorporation of the heaviest REE. However, the three sites available for REE incorporation in amphibole may be combined with different weights

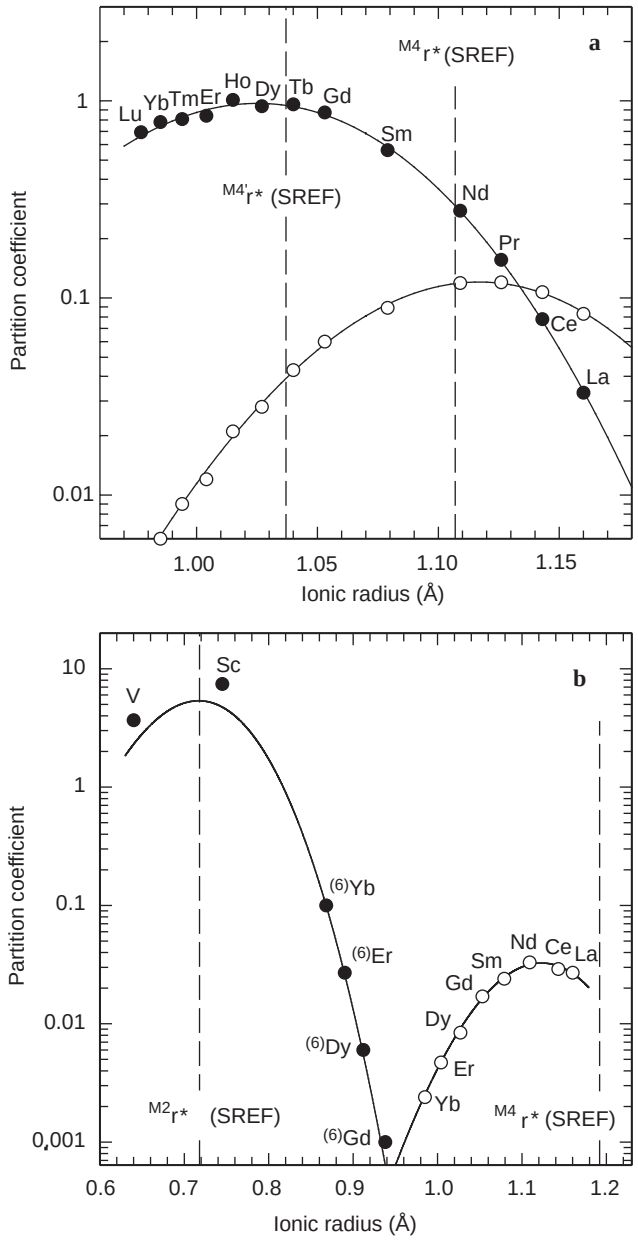

Fig. 4 REE partition coefficients versus cation radius for **a** the two sites within the M4 cavity in kae 4722–13a and **b** the two M2 and M4 sites in K-ric RB31–1. The curves represent Blundy and Wood's (1994) Eq. (2) for each site; r_0, D_0 and E values are reported in Table 3, whereas the observed dimensions from SREF are shown (*dashed lines*). *Open* and *filled circles* correspond to the contribution of each site (A and B respectively). The distinct contributions to the total D measured for an element (D_{meas}) were calculated using the theoretical values of the curves relative to each site at the ionic radius of the element (D_A and D_B) as $D_A/(D_A + D_B) \times D_{meas}$ and $D_B/(D_A + D_B) \times D_{meas}$, respectively

in different compositions, thus determining the features of a complex partition coefficient pattern for REE. The pattern shown by par RB52–3 is affected by both the contribution of the M2 octahedron and the displacement of the vertex of the M4 parabola towards smaller values due to the presence of some (albeit very low) cummingtonite component (Fig. 3 and Table 3).

It is also worthy of note that high values for REE partition coefficients are observed in amphiboles only if suitable sites (M4′ and/or M2, i.e. substitution after Mg or Fe^{2+}) are available, and that the contribution of the M4 site (substitution after Ca) is always quite low. The relatively high $^{Amph/L}D$ for middle and heavy REE observed by some authors (Andreessen et al. 1996; Klein et al. 1997), therefore, are most likely related to the amount of the cummingtonite component, i.e. to the incorporation of REE into M4′, which makes up more than 90% of the total content of MREE and HREE in kae 4722–13a.

Implications of the ordering of REE for predictive models

When REE enter two distinct sites with distinct crystal-chemical mechanisms (i.e. M4 and M2, as in K-ric RB31–1), the use of predictive models based on single-site incorporation leads to incorrect results. In particular, the prediction of D_{HREE} is strongly underestimated. The contribution of the octahedra to D can be very subordinate, as in the case of kae 4722–13a, but has to be taken into account, at least when the cummingtonite component is low.

When REE partition themselves between two distinct sites within a cavity (i.e. M4 and M4′), thus contributing to the same crystal-chemical mechanism, a smooth single curve is obtained for the partition coefficient pattern. This is because the dimensions and the compliance of the two co-ordination polyhedra are more similar. There are two ways to estimate r_0 in predictive models of mineral/melt partitioning based on the elastic-strain theory: (1) r_0 is derived independently from SREF on the same crystal or crystals of similar composition and from crystal-chemical considerations, and (2) r_0 is calibrated against the mineral major element composition by fitting sets of experimental partition coefficient data to a single curve centred around the dominant constituent.

In the former case, an incorrect assignment of the dominant structural site would introduce significant errors. With respect to kae 4722–13a, if partition coefficients had been predicted with a single curve of r_0 close to r* or to r_{Ca}, the ratio of the partition coefficient of an LREE to an HREE would have been significantly overestimated. Therefore, the REE fractionation assumed in geochemical modelling would have been incorrect. The second method is sounder because the input value of r_0 would be properly assigned if the composition of the modelled mineral falls within the interval of calibration of r_0. Also the D_{REE} pattern predicted on the basis of a single curve would be in agreement with the measured ones. When calibrating r_0, an increasing importance of the M4′ site relative to M4 would appear as a decrease in the calculated value for r_0. A variation of r_0 with the ionic charge has been recently observed when fitting the partitioning data for clinopyroxene and gar-

net under the constraints of a single site (J. Blundy, personal communication; van Westrenen et al. 1999). It is most likely that the considerations reported above provide a plausible explanation for this phenomenon. A variation of r_0 with the ionic charge is related to the different proportions of the sites suitable for incorporation of trace elements with different ionic charges. Finally, it is also worth noting that an incorrect site-assignment for REE affects the estimate of the Young's modulus.

When combined with independent estimates of polyhedral dimensions, the elastic-strain model allows linkage of fine-scale site preference to the macroscopic properties of minerals, giving further constraints for more reliable predictive models of mineral/melt partitioning. The preference of REE for polyhedra with smaller size and lower co-ordination than those occupied by Ca invalidates the general idea that Ca acts as the "carrier" for REE.

The combined approach reported in this work allowed us to unravel the complex mechanisms of REE incorporation in amphibole. We are aware that the results of this work cannot be readily applied to the calibration of predictive models in the absence of accurate structure refinements and thus of reliable site populations for major elements. Accurate electron microprobe analyses usually allow the cummingtonite component to be evaluated, but since correct unit formulae can be obtained for pargasite/kaersutite and richterite only in the absence of dehydrogenation, care must be taken when the Ti content exceeds 0.15 apfu. Nevertheless, we provide evidence that distinct ordering patterns for REE can be recognised from the shape of the Onuma curves constructed from accurately determined $^{Amph/L}D_{REE}$. D_{Yb}/D_{Dy} close to unity indicates the contribution of two different sites within the M4 cavity, whereas D_{Yb} significantly larger than D_{Dy} implies REE partitioning between M4 ($\pm$M4′) and M2.

The mechanisms of REE incorporation described in this work are likely to be applicable to other rock-forming minerals in which alternative co-ordinations within the same structural sites have been observed for (Mg, Fe^{2+}) and for Ca (e.g. clinopyroxene, Rossi et al. 1987; garnet, Quartieri et al. 1995). In particular, because of its importance in geochemical investigations and modelling, we emphasise that the crystal-chemical behaviour of clinopyroxene is very similar to that of amphibole, at least as far as the relevant sites for REE incorporation are concerned ($M4_{amph} \leftrightarrow M2_{cpx}$, $M4'_{amph} \leftrightarrow M2'_{cpx}$, $M2_{amph} \leftrightarrow M1_{cpx}$). Distinct ordering patterns are therefore likely to occur in clinopyroxene.

Acknowledgements Maria Pia Riccardi (CGS, Pavia) and Marco Palenzona (CNR-CSCC, Pavia) are acknowledged for their help during EMP and SIMS analyses, respectively. Simon Jackson (Macquarie University, Sydney) is gratefully acknowledged for advice on laser-ablation analysis. This paper greatly benefited from constructive comments by Trevor Green, Frank Hawthorne and Roger Nielsen. Funding was provided by Consiglio Nazionale delle Ricerche, Ministero dell'Università e della Ricerca Scientifica e Tecnologica (MURST) and by Deutsche Forschungsgemeinschaft grant Fo 181/9.

References

Adam J, Green TH (1994) The effect of pressure and temperature on the partitioning of Ti, Sr, and REE between amphibole, clinopyroxene and basanitic melts. Chem Geol 117: 219–233

Andreessen T, Bottazzi P, Vannucci R, Mengel K, Johannes W (1996) Experimental determination of trace element partitioning between amphibole and melt. J Conf Abstr 1: 17

Andronikov AV, Egorov LS (1993) Mesozoic alkaline-ultramafic magmatism of Jetty Peninsula. In: Findlay RH, Unrug R, Banks MR, Veevers JJ (eds) Gondwana Eight, assembly, evolution and dispersal. Balkema, Rotterdam, pp 547–557

Beattie P (1994) Systematics and energetics of trace-element partitioning between olivine and silicate melts: implications for the nature of mineral/melt partitioning. Chem Geol 117: 57–71

Blundy J, Wood B (1994) Prediction of crystal-melt partition coefficients from elastic moduli. Nature 372: 452–454

Bottazzi P, Ottolini L, Vannucci R, Zanetti A (1994) An accurate procedure for the quantification of rare earth elements in silicates. In: Benninghoven A, Nihei Y, Shimizu R, Werner HW (eds) Secondary ion mass spectrometry – SIMS IX. Wiley, Chichester, pp 927–930

Brenan JM, Shaw HF, Ryerson FJ, Phinney DL (1995) Experimental determination of trace-element partitioning between pargasite and a synthetic hydrous andesitic melt. Earth Planet Sci Lett 135: 1–12

Brice JC (1975) Some thermodynamic aspects of the growth of strained crystals. J Cryst Growth 28: 249–253

Brumm R (1998) Die experimentelle Bestimmung von Amphibol/Schmelze-Verteilungskoeffizienten in lamproitischen und lamprophyrischen Systemen. Dr. rer. nat. Dissertation, University of Göttingen, 132 pp

Brumm R, Foley SF, Tiepolo M, Vannucci R (1999) Trace element partitioning in amphiboles: implications for magma genesis and magma composition. EUG 10, Strasbourg. J Conf Abstr 4: 356

Dalpé C, Baker DR (1994) Partition coefficients for rare-earth elements between calcic amphibole and Ti-rich basanitic glass at 1.5 GPa, 1100 °C. Mineral Mag 58A: 207–208

Foley SF, van der Laan SR, Horn I (1996) Major- and trace element compositions of melts from mica-clinopyroxenite in the lower cratonic lithosphere – results of experiments on mantle vein assemblages. J Conf Abstr 1: 172

Foley SF, Brumm R, Tiepolo M, Bottazzi P, Oberti R, Vannucci R, Zanetti A (1999) HFSE site preferences and coupled/decoupled behaviour of Ti, (Nb,Ta) and (Zr,Hf) in amphiboles. 1999 Spring AGU Meeting, Boston. EOS, Trans Am Geophys Union 80: S360

Hack PJ, Nielsen RL, Johnston AD (1994) Experimentally determined rare-earth element partitioning behavior between clinopyroxene and basaltic liquids at pressure up to 20 Kbar. Chem Geol 117: 89–105

Harte B, Kirkley M (1997) Partitioning of trace element between clinopyroxene and garnet: data from mantle eclogites. Chem Geol 136: 1–24

Klein M, Stosch H-G, Seck HA (1997) Partitioning of high field-strength and rare-earth elements between amphibole and quartz-dioritic to tonalitic melts: an experimental study. Chem Geol 138: 257–271

LaTourrette T, Hervig RL, Holloway JR (1995) Trace element partitioning between amphibole, phlogopite, and basanite melt. Earth Planet Sci Lett 135: 13–30

Longerich HP, Jackson SE, Günther D (1996) Laser ablation inductively coupled plasma mass spectrometric transient signal data acquisition and analyte concentration calculation. J Anal At Spectrom 11: 899–904

Nagasawa H (1966) Trace element partition coefficient in ionic crystals. Science 152: 767–769

Oberti R, Ghose S (1993) Crystal-chemistry of a complex Mn-bearing alkali amphibole (''tirodite'') on the verge of exsolution. Eur J Mineral 5: 1153–1160

Oberti R, Ungaretti L, Cannillo E, Hawthorne FC (1992) The behaviour of Ti in amphiboles: four- and six-co-ordinated Ti in richterite. Eur J Mineral 4: 425–439

Oberti R, Vannucci R, Zanetti A, Tiepolo M, Brumm RC (1999a) On the correct determination of D_{Ti} in Amph/liq and Amph/Cpx partitioning: the key-role of the crystal-chemical mechanisms. Am Mineral

Oberti R, Hawthorne FC, Camara F, Raudsepp M (1999b) Unusual M^{3+} cations in synthetic amphiboles with nominal fluoro-eckermannite composition: deviations from stoichiometry and structural effects of the cummingtonite component. Am Mineral 84: 102–111

Onuma N, Higuchi H, Wakita H, Nagasawa H (1968) Trace element partition between two pyroxenes and the host lava. Earth Planet Sci Lett 5: 47–51

Ottolini L, Bottazzi P, Zanetti A, Vannucci R (1995) Determination of hydrogen in silicates by secondary ion mass spectrometry. Analyst 120: 1309–1313

Purton JA, Allan NL, Blundy JD, Wasserman EA (1996) Isovalent trace element partitioning between minerals and melts: a computer simulation study. Geochim Cosmochim Acta 60: 4974–4987

Quartieri S, Chaboy J, Merli M, Oberti R, Ungaretti L (1995) Local structural environment of calcium in garnets: a combined structure-refinement and XANES investigation. Phys Chem Miner 22: 159–169

Rossi G, Oberti R, Dal Negro A, Molin GM, Mellini M (1987) Residual electron density at the M2 site in *C*2/*c* clinopyroxenes: relationships with bulk chemistry and sub-solidus evolution. Phys Chem Miner 14: 514–520

Ryerson FJ, Hess PC (1978) Implications of liquid-liquid distribution coefficients to mineral-liquid partitioning. Geochim Cosmochim Acta 42: 921–932

Shannon RD (1976) Revised effective ionic radii and systematic studies of interatomic distances in halides and chalcogenides. Acta Crystallogr 32 A: 751–767

Sweeney RJ, Green DH, Sie SH (1992) Trace and minor element partitioning between garnet and amphibole and carbonatitic melt. Earth Planet Sci Lett 113: 1–14

Taylor RP, Jackson SE, Longerich HP, Webster JD (1997) In situ trace-element analysis of individual silicate melt inclusions by laser ablation microprobe – inductively coupled plasma – mass spectrometry (LAM-ICP-MS). Geochim Cosmochim Acta 61: 2559–2567

Tiepolo M (1999) Determinazione sperimentale dei coefficienti di distribuzione solido/liquido in anfiboli di mantello: ruolo del controllo cristallochimico. PhD Thesis, Università di Pavia, 314 pp

Tiepolo M, Zanetti A, Oberti R (1999) Detection, crystal-chemical mechanisms and petrological implications of $^{[6]}Ti^{4+}$ partitioning in pargasite and kaersutite. Eur J Mineral 11: 345–354

van der Laan SR, Foley SF (1994) MARIDs and mantle metasomatism. Mineral Mag 58 A: 505–506

van Westrenen W, Blundy J, Wood B (1999) Crystal-chemical controls on trace element partitioning between garnet and anhydrous silicate melt. Am Mineral 84: 838–847

Wedepohl KH (1983) Die chemische Zusammensetzung der basaltischen Gesteine der nordlichen Hessichen Senke und ihrer Umgebung. Geol Jahrb Hessen 111: 261–302

Wood BJ, Blundy JD (1997) A predictive model for rare earth element partitioning between clinopyroxene and anhydrous silicate melt. Contrib Miner Petrol 129: 166–181

Yang H, Konzett J, Prewitt CT, Fei Y (1999) Single-crystal structure refinement of synthetic ^{M4}K-substituted potassic richterite, $K(KCa)Mg_5Si_8O_{22}(OH)_2$. Am Mineral 84: 681–684